

## RESEARCH ARTICLE

10.1002/2016JC011800

## Numerical modeling of intrinsically and extrinsically forced seasonal circulation in the China Seas: A kinematic study

Jianping Gan<sup>1</sup>, Zhiqiang Liu<sup>1</sup>, and Linlin Liang<sup>1</sup><sup>1</sup>Department of Mathematics and Division of Environment, Hong Kong University of Science and Technology, Hong Kong, China

## Key Points:

- We developed a novel circulation model for the entire China Seas that considered the linked forcings of winds, tides, and external fluxes
- The circulation in the China Seas is forced intrinsically by the wind-forced current and extrinsically by exchange flow with adjacent oceans
- The circulation in the China Seas can be characterized by rotating layered circulation

## Correspondence to:

J. Gan,  
magan@ust.hk

## Citation:

Gan, J., Z. Liu, and L. Liang (2016), Numerical modeling of intrinsically and extrinsically forced seasonal circulation in the China Seas: A kinematic study, *J. Geophys. Res. Oceans*, 121, doi:10.1002/2016JC011800.

Received 16 MAR 2016

Accepted 4 JUN 2016

Accepted article online 9 JUN 2016

**Abstract** We developed a new three-dimensional, high-resolution ocean circulation model for the entire China Seas (CS) region. The model considered the linked physics associated with the western boundary current, monsoonal wind, and tidal forcings, and topography in both the CS and the adjacent oceans. From this well-validated model, we derived new insights into the three-dimensional seasonal circulation of the CS in response to the intrinsic forcing of monsoonal winds and extrinsic forcing of flow exchange with adjacent oceans through the straits and over the slope around the periphery of the CS. Besides the East Asian monsoon forcing, we found that the extrinsic forcings interact coherently with each other and with the interior circulation to jointly shape the CS circulation. Specifically, we revealed rotating layered circulation in the CS. The circulation in the South China Sea has a vertical cyclonic-anticyclonic-cyclonic pattern in the upper-middle-lower layers, which we relate to the inflow-outflow-inflow transport in those layers in the Luzon Strait. The circulation in the East China Sea (ECS) is characterized by a vertically variable cyclonically rotating flow, and the circulation in the Yellow Sea (YS) is represented by a cyclonic movement in the upper layer and an anticyclonic movement in the lower layer. We attribute the cross-shelf variation of the along-shelf current to the ECS circulation pattern, while the vertically variable intrusive current at the central trough, together with the seasonally varied west and east coastal currents, shape the two-layer circulation in the YS.

## 1. Introduction

The marginal South China Sea (SCS) and the shelf seas of the Bohai Sea (BHS), Yellow Sea (YS), and East China Sea (ECS) are linked together by the Taiwan Strait (TWS) to form the China Seas (CS, Figure 1). The CS are connected to the Western Pacific Ocean (WPO) by the continental slope off the ECS and by the Luzon Strait (LS) to the east of the SCS. The CS are also connected to the Sea of Japan by the Tsushima Strait, to the Java Sea by the Karimata Strait, and to the Sulu Sea by the Mindoro Strait and Balabac Strait (Figure 1). The deep SCS basin and broad continental shelves of the ECS, BHS, and YS and the SCS characterize the CS topography. The steep continental slope links the shelves with the deep basin. We summarized all abbreviations that have been commonly used in the CS in Table 1.

The circulation in the CS is largely governed by the dynamics of the East Asian monsoon wind-driven flow, external flow from adjacent oceans, and the interaction of these flows with topography. In the SCS, the basin circulation is predominately shaped by cyclonically and anticyclonically circulating flows along the slope at the continental margin. These flows in the SCS are the response to winter northeasterly and summer southwesterly monsoonal winds, and Kuroshio intrusion from LS [Qu, 2000; Xue *et al.*, 2004; Gan *et al.*, 2006]. In the ECS, monsoonal winds, tides, Kuroshio intrusion, and freshwater discharged from the Changjiang River (Figure 1) yield the typical shelf circulation [e.g., Fang *et al.*, 1991; Guo and Yanagi, 1998; Liu and Gan, 2012]. The circulations in the BHS and the YS are circular due to the wind and external flux forcings in semiclosed shelf seas [e.g., Isobe, 2008]. All these circulations in different seas have strong seasonal and spatial variability that respond to changes in local wind and external forcings over the highly variable topography of the CS.

The exchange flow through the LS, between the SCS and the Kuroshio in the WPO, is the most important extrinsic forcing to the CS. This flow has a net annual westward transport [e.g., Gan *et al.*, 2006; Hsin *et al.*, 2012], and also has a sandwich-like flow pattern in the water column. The intrusive currents occupy an upper layer ( $\sim < 750$  m) and a deeper layer ( $> 1500$  m) and the extrusive currents occupy a middle layer in

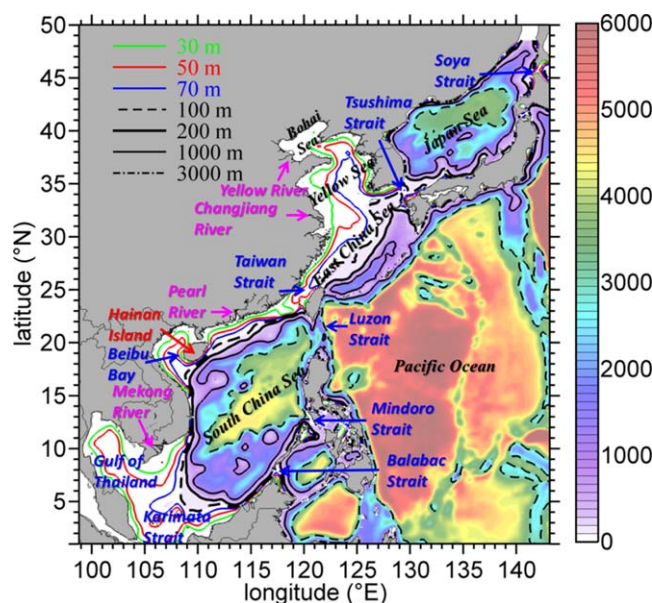


**Figure 1.** Model computational domain and bathymetry (m, color contours) with the 30, 50, 70, 100, 200, 1000, and 3000 m isobaths shown by respective contour lines. The locations of seas, islands, rivers, and straits are marked in the map.

between. A large uncertainty exists in the estimate of the annual mean transport through LS, which ranged from 0.5 to 10 Sv [e.g., Xue *et al.*, 2004; Hsin *et al.*, 2012]. We expect that the exchange flow through the LS importantly shapes the three-dimensional circulation in the SCS, and even in the entire CS, although we have not established a complete kinematical and dynamical rationalization.

The transport through the TWS, which is in the central part of the CS, dynamically links the circulation in the ECS with that in the SCS. The wind-driven shelf currents over the connected shelves in these two seas strongly determine the transport in the TWS. In addition, the northward-turning intrusive water from the Kuroshio that flows through the LS [Qiu *et al.*, 2011] and the northward Taiwan Warm Current (TWWC) that occupies the broad

ECS coastal waters [Guan and Fang, 2006] also affect the flow field in the TWS. The annual mean TWS transport is northward and its magnitude ranges from ~1 to ~2 Sv [e.g., Fang *et al.*, 1991; Jan and Chao, 2003]. The exchange transport through the TWS acts as the external inflow/outflow forcing for the ECS and SCS and importantly regulates the Kuroshio intrusion over the slope to the east of the ECS and the Tsushima warm current to the north of the ECS [Guo *et al.*, 2006].

In the ECS, the Kuroshio intrusion has an annual net transport of ~1.4 Sv and is important to determine the shelf circulation [Guo *et al.*, 2006]. The intrusion occurs when the Kuroshio at its shore-side boundary (SSB) crosses the isobaths and intrudes into the ECS [Liu and Gan, 2012]. The intrusion is expected to be controlled by the local dynamics arising from the interaction between the Kuroshio and slope topography [Gan *et al.*, 2013]. Because of the annual net inflows from the TWS and Kuroshio intrusion into the ECS, the annual mean transport in the Tsushima Strait is directed northward year round and has a magnitude of ~2.64 Sv with notable seasonal variability [Takikawa *et al.*, 2005].

Away from the dynamically active Kuroshio-influenced region in the SCS, inflow/outflow transports in the Mindoro Strait and Karimata Strait respond interactively to both the intrusion of the Kuroshio in the LS and the SCS circulation. The main intrusive transport from the LS exits through the Mindoro Strait with a mean transport of ~2.4 Sv [Qu and Song, 2009]. The transport from the LS inflow also exits the Karimata Strait with an annual mean transport of 1 Sv [Fang *et al.*, 2010].

Clearly, these exchange flows between the seas within the CS and between the CS and adjacent oceans interactively regulate the circulation in the CS. However, we know little about the three-dimensional, time

**Table 1.** Abbreviations Used in the Paper

Seas/Straits	Abbreviations	Currents	Abbreviations
Bohai Sea	BHS	Cyclonical-anticyclonical-cyclonical circulation	CACC
China Seas	CS	North Equatorial Current	NEC
East China Sea	ECS	South China Sea Through Flow	SCSTF
Luzon Strait	LS	Taiwan Warm Current	TWWC
South China Sea	SCS	West Korea Current	WKC
Taiwan Strait	TWS	Yellow Sea Warm Current	YSWC
Western Pacific Ocean	WPO	Yellow Sea Coastal Current	YSCC
Yellow Sea	YS		

dependence of these flows, in particular the response of CS circulation to the interaction between the wind-driven circulation and these flows over the complex topography.

The circulations in the individual seas of the CS have been extensively studied, particularly the wind-forced circulation. However, these seas are topographically and physically connected among themselves and with adjacent oceans, and these connections exert their influences mainly through the water exchanges through transports in the straits/slope surrounding the CS. This extrinsic forcing interacts with the intrinsic circulation to jointly govern the overall circulation in the entire CS system and in the individual seas as well. The characteristics of the circulation in the CS with regards to the dynamic connections of the seas and to the extrinsic and intrinsic forcings have rarely been investigated. In this study, we developed a novel three-dimensional model and reported new insights into the circulation in responses to these connections and forcings in the CS.

## 2. Ocean Model and Implementations

We used the Regional Ocean Modeling System (ROMS) [Shchepetkin and McWilliams, 2005] to model the three-dimensional, time-dependent circulation governed by the hydrostatic primitive equations. For the vertical mixing parameterization, we adopted the local closure scheme of Mellor and Yamada [1982] which is based on the level-2.5 turbulent kinetic energy equations.

The model domain extended from  $\sim 0.95^{\circ}\text{N}$ ,  $99^{\circ}\text{E}$  in the southwest corner to the northeast corner of the Sea of Japan (Figure 1). This computation domain provided a high degree of dynamic freedom for the western boundary current (Kuroshio) and for transport/exchange flow through the major straits/slope surrounding the CS to be developed by the model physics of the primitive equations. We adopted a curvilinear grid with a (430, 550) dimensional array for the horizontal coordinates ( $x, y$ ). The horizontal size of this grid array decreased gradually from  $\sim 10$  km in the southern part to  $\sim 7$  km in the northern part of the domain. Vertically, we adopted a 30-level stretched generalized terrain-following coordinate ( $s$ ). The vertical grid spacing had a higher resolution in the surface and bottom boundary layers and avoided artificial diffusion in large water depths. We obtained water depths  $h(x, y)$  by merging ETOPO5 ( $1/12^{\circ}$ ) data from the National Geophysical Data Center in the U.S. with digitized water depths from navigation maps published by the China Maritime Safety Administration. Our limited-area simulation considered the physical and numerical needs of resolving circulation dynamics in the CS which would have been difficult for a global-scale model to achieve.

We forced the model with wind stress derived from climatological (averaged from 1988 to 2013) monthly Reanalysis of 10 m Blended Sea Winds released by the National Oceanic and Atmospheric Administration (<https://www.ncdc.noaa.gov/oa/rsad/air-sea/seawinds.html>), based on the bulk formulation by Fairall *et al.*

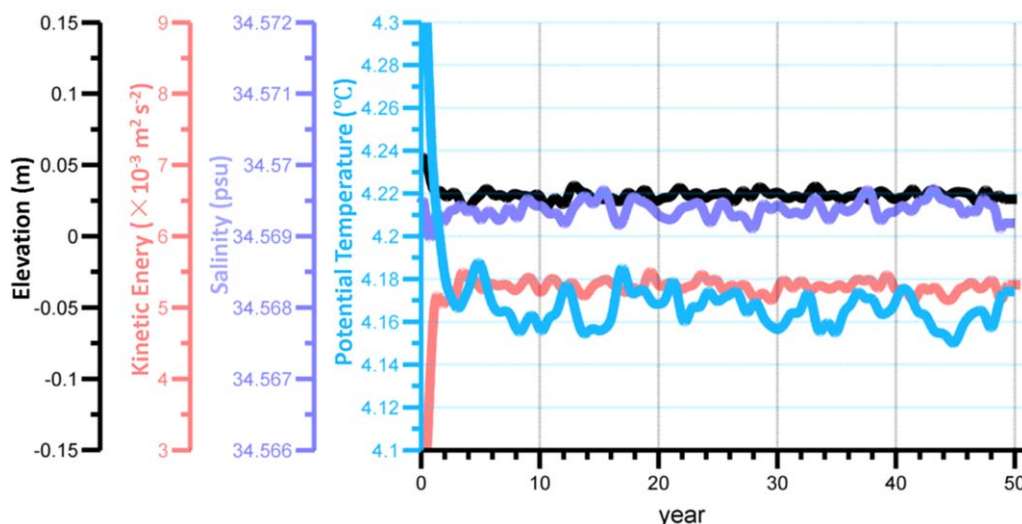
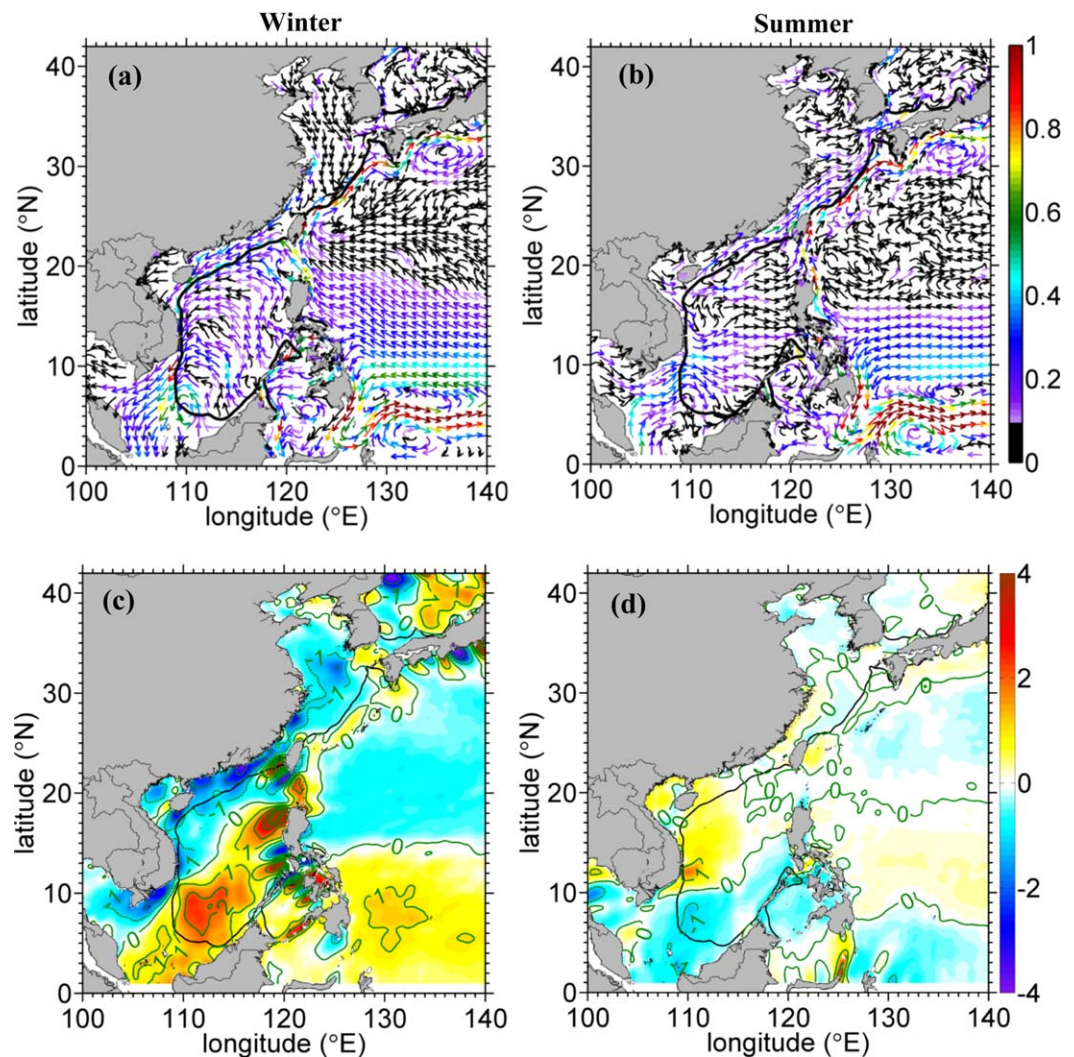


Figure 2. Time series of the domain-averaged surface elevation (m), kinetic energy ( $\text{m}^2 \text{s}^{-2}$ ), potential temperature ( $^{\circ}\text{C}$ ), and salinity.



**Figure 3.** (a, b) Surface velocity vectors ( $\text{m s}^{-1}$ ) and (c, d) wind stress curl ( $10^{-7} \text{ Pa m}^{-1}$ ) in the CS during winter and summer. The black solid line marks the 200 m isobath.

[2003]. The data set has  $0.25^\circ \times 0.25^\circ$  resolution. We calculated the atmospheric heat and salt fluxes from climatological monthly mean NCEP (National Centers for Environmental Prediction) Reanalysis 1 meteorological variables using bulk formula. The Reanalysis has  $\sim 1.875^\circ$  resolution.

We applied active open boundary conditions (OBCs), which integrated the active OBCs of Gan and Allen [2005] and the Flather-type OBCs [Flather, 1976], to accommodate concurrently tidal and subtidal forcing along the eastern and southern open boundaries of the model domain. The OBCs linked the CS processes with the remote forcing, and they allowed disturbances from the interior of the CS to propagate outward freely. The OBCs also separated all subtidal components into local (forced) and global (unforced) components such that inflow/outflow conditions can be calculated with the unforced Orlandi-type OBCs using the global component. The local components of eastward and westward depth-integrated velocities ( $U$ ,  $V$ ), depth-dependent velocities ( $u$ ,  $v$ ), temperature ( $T$ ), and salinity ( $S$ ) along the open boundaries were the monthly mean solutions derived from the Ocean General Circulation Model for the Earth Simulator (OFES) global model [Sasaki et al., 2008]. This global model has  $10 \text{ km} \times 10 \text{ km}$  horizontal resolution and is forced with climatological monthly mean atmospheric fluxes. The same OBCs were applied to  $U$ ,  $V$ ,  $u$ ,  $v$ ,  $T$ , and  $S$  for dynamic consistency.

Tidal forcing exerts its effect on the CS through the tidal wave propagation from the WPO. We applied the tidal forcing, with eight harmonic constituents ( $M_2$ ,  $S_2$ ,  $N_2$ ,  $K_2$ ,  $K_1$ ,  $O_1$ ,  $P_1$ , and  $Q_1$ ), derived from the Pacific

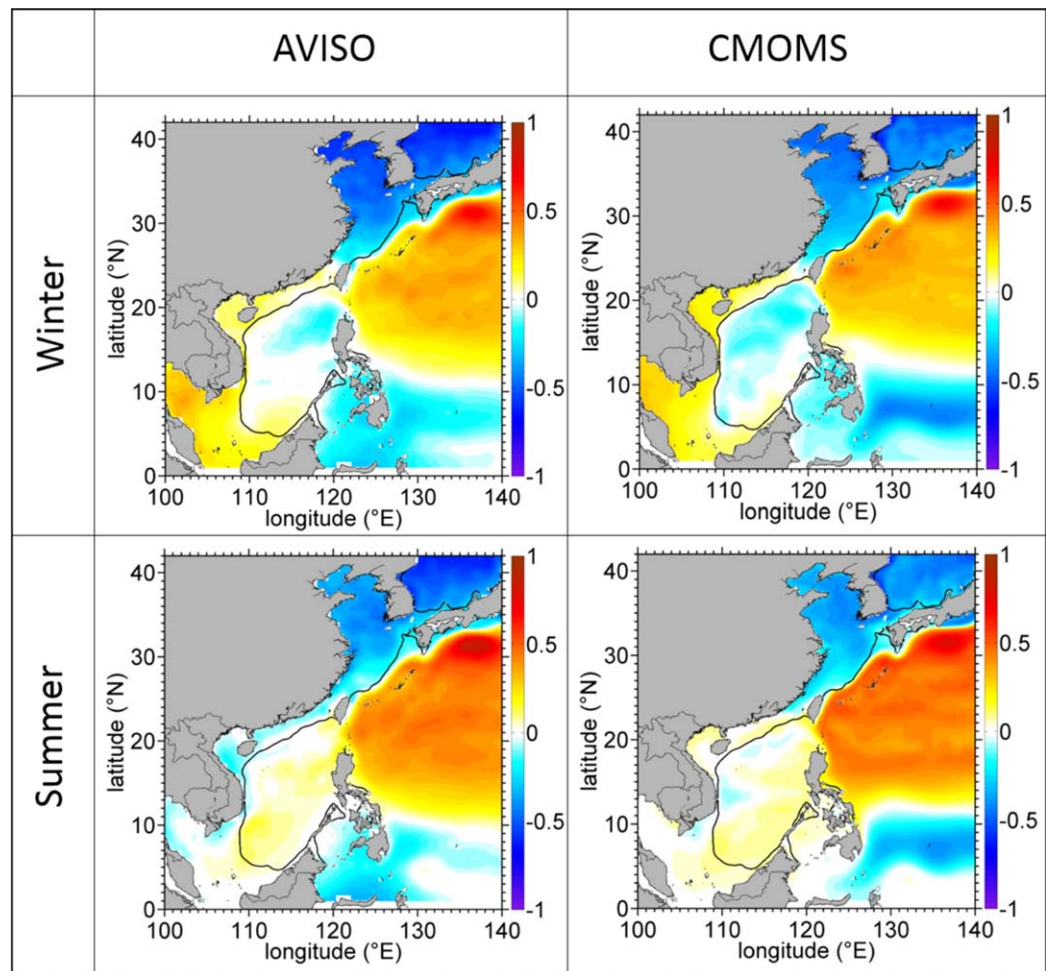


**Figure 4.** Mean absolute dynamic topography (ADT in m, averaged from 1993 to 2012) from AVISO and model results in winter and summer. Additional values of  $h_0$  have been subtracted from the AVISO data. The black solid line marks the 200 m isobath.

Ocean and Indian Ocean subdomains of the Inverse Tide Model (ITM) [Egbert *et al.*, 1994] as boundary forcing in our model. The ITM is constrained by TOPEX/Poseidon altimetry data and uses an advanced and effective data assimilation technique. In addition, in our model, we added tidal potential to a pressure term in momentum equation, following Ray [1998], to account for the self-attraction and loading effect of the ocean. We used the climatological monthly discharges from major rivers (e.g., the Mekong River, Pearl River, and Changjiang River) and other smaller rivers in the Gulf of Beibu, BHS, and YS as lateral buoyancy fluxes. We obtained the discharge data from the Information Center of Water Resources (Bureau of Hydrology, Ministry of Water Resources of P. R. China) and from those reported in literatures [e.g., Dai and Trenberth, 2002].

We initialized our model with winter climatological WOA13 (World Ocean Atlas 2013) potential temperature and salinity, and spun the model up for 50 years. To avoid a drifting ( $T$ ) and ( $S$ ) in the deep ocean [Gan *et al.*, 1998], we relaxed ( $T$ ,  $S$ ) in the bottom layers of the deep basin ( $h > 200$  m) to the seasonally averaged values from WOA13 in 200 days. We also applied same relaxation to  $S$  in the upper layer of the deep basin to compensate for the uncertainty in surface salinity flux arising from NCEP Reanalysis precipitation data.

The CS circulation model is part of the China Sea Multi-Scale Ocean Modeling System (CMOMS) that integrates circulation in estuary/shelf/basin/open oceans of different subscales. The numerical implementations of the CMOMS consider regional ocean circulation dynamics by adopting the physically sensible computational domain, regionally validated atmospheric and lateral (both mechanical and thermodynamic) forcings, and numerically and physically adaptable OBCs.

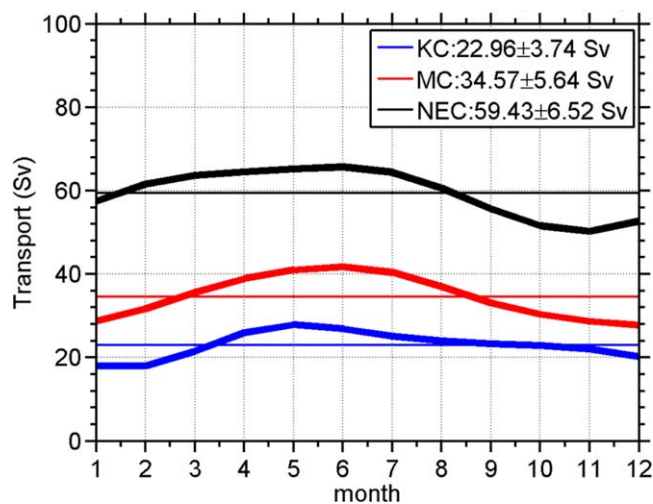


**Figure 5.** Time series of transports (Sv) in the NEC (black) across meridional section along 135°E between 8°N and 20°N, the Kuroshio (blue) across zonal section along 20°N, and the Mindanao Current (red) across zonal section along 8°N from the coast to 135°E from the model. The westward current in the NEC, the northward current in the Kuroshio, and the southward current in the Mindanao Current in the upper 400 m are used to calculate their respective transports. Their annual mean values and standard deviations are also shown.

shown by surface velocity vectors in Figure 3 and by satellite remotely sensed absolute dynamic topography (ADT) distributed by the AVISO (Archiving, Validation and Interpretation of Satellite Oceanographic) by model result in Figure 4. The AVISO data are averaged from 1993 to 2012.

The northeasterly and southwesterly monsoonal wind-forced circulation in the CS is mainly shaped by Ekman transport in the shallow shelf regions and by circular motion excited by seasonally opposite wind stress curls in the deep basin (Figure 3). These are relatively well known [e.g., *Qu*, 2000; *Xue et al.*, 2004; *Gan et al.*, 2006, 2009a; *Liu and Gan*, 2015]. However, the effects of external forcing from adjacent oceans and the interaction of the external forcing with the wind-forced currents in the CS are not as well understood.

Our results show that the exchange flows around the periphery of the CS associate largely with the current system in the tropical WPO. The surface North Equatorial Current (NEC) flows westward between 8°N and 18°N, and it bifurcates east of the Philippines at ~11°N at the surface in summer (June, July, and August), and at ~14°N in winter (December, January, and February), as shown by seasonal velocity fields (Figure 3) and ADT (Figure 4). The annual mean transport of the NEC is ~59 Sv (Figure 5). Large variation of mean NEC transport has been estimated to be ranged from ~57 Sv [*Qiu and Lukas*, 1996] to ~40 Sv [*Qu et al.*, 1998]. All the previous estimates were derived geostrophically from the spatiotemporally limited hydrographic measurements or were from numerical model-based results. On average, the northward and southward bifurcation of the NEC form the northward Kuroshio of ~23 Sv and the southward Mindanao Current of ~35 Sv, respectively (Figure 5). These two values, obtained from the CMOMS, are close to the transport estimates by *Qiu and Lukas* [1996], but Kuroshio transport is larger than the recent field measurement by *Lien et al.* [2014]. Our transports presented here were integrated upward from the depth of 400 m similar to *Qiu and Lukas* [1996]. It should be noted that Kuroshio transport varies greatly in space and time [*Jan et al.*, 2015], as a result of inter-annual variability and variable local forcing along its path. The seasonal phases of NEC, Kuroshio, and Mindanao Current are similar to those described in *Qu et al.* [1998], *Yaremchuk and Qu* [2004], and *Qu et al.* [2012]. As a result of decreasing transport in the NEC and the northward shifting NEC from summer to winter, smaller Kuroshio transport (Figure 5) but stronger westward intrusions of Kuroshio occur in winter (also see section 5). These intrusions include the Kuroshio entering the SCS through the LS [*Qu et al.*, 2000] and into the ECS along the edge of the ECS shelf [*Liu and Gan*, 2012].

Over the CS, the SCS exhibits a basin-wide cyclonic (anticyclonic) circulation with a distinct low (high) ADT that is centered in the deep basin ( $h > 200$  m) in winter (summer) (Figure 4). In the shelf seas (ECS and YS), the ADT increases southward along the shelf and it manifests as an intrinsic northward pressure gradient

The time series of the domain-averaged surface elevation, kinetic energy (KE), salinity, and potential temperature (Figure 2) show that the ocean reaches a statistical equilibrium within ~5 years. The fact that the dynamic and thermodynamic fields in the model are able to reach an equilibrium state also suggests that the model is reasonably well implemented and that the OBCs perform stably. We used average values of model variables in the last 5 years of the 50 year integration for the analyses in our study.

### 3. General Physical Characteristics

#### 3.1. Circulation and Variability

The seasonal circulation, forced by both the East Asian monsoon wind forcing and the intrusive currents over the unique topography of the CS, is

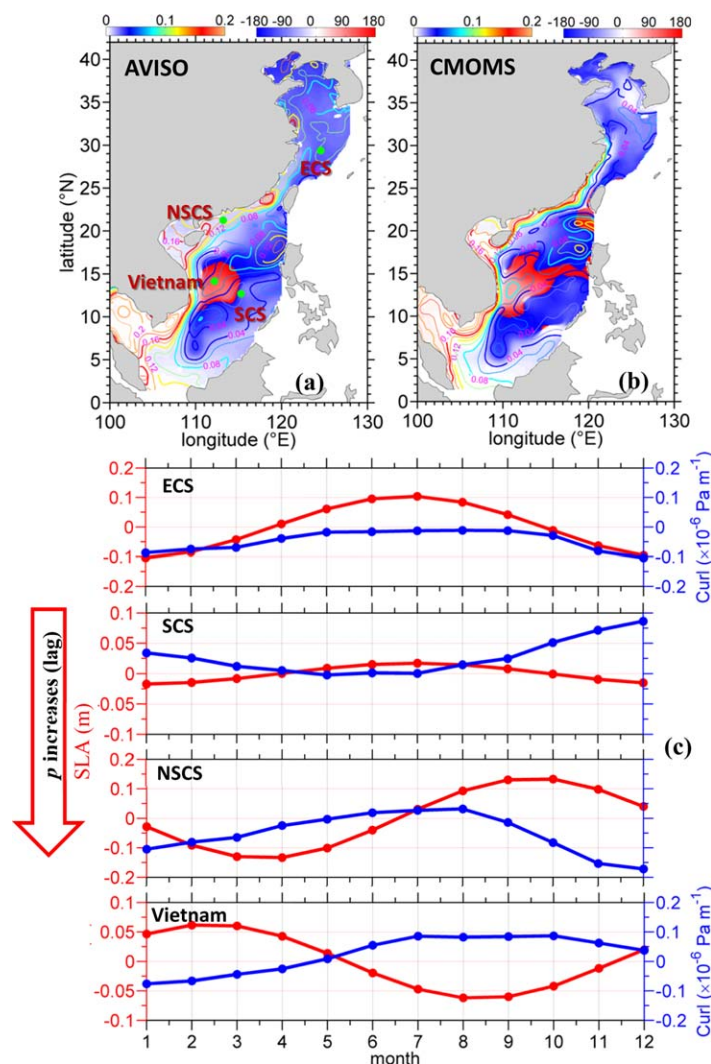


**Figure 6.** Harmonic analysis of SLA seasonality in the CS. The contour lines and color contours showed the amplitude ( $A$ , meter, left color bar) and phase-lag ( $p$ , degree, right color bar) of SLA from (a) observation and (b) model, respectively.  $p > 0$  and  $p < 0$  represent a time lag and advance ( $\sim 1$  d/degree, relative to a reference time 1 January) of the SLA seasonal variation over a period of 1 year, respectively. (c) The time series of SLA and wind stress curl in stations marked in Figure 6a.

This decrease indicates relatively weak seasonality far from the shelf regions. We associate the large amplitude ( $> 0.08$  m) west of the Luzon Island with the seasonal western Luzon eddy [Wang and Gan, 2014]. Similarly, we link  $A > 0.04$  m east of Vietnam to the variation of the seasonal eddy arising from recirculation in the coastal current separation [Gan and Qu, 2008].

The negative cophase ( $p < 0$ ) in broad region of the CS, small positive  $p$  in the shelf waters, and positive  $p$  east of the central Vietnam indicate sequentially the temporal variation of SLA in these regions (Figures 6a and 6b). Combined with the time series of SLA in Figure 6c, these findings show that the seasonal SLA signals in the central basin (e.g., station SCS) and in the outer ECS shelf (e.g., ECS station) occur  $\sim 3$ – $4$  months ( $p$  between  $-90^\circ$  and  $-120^\circ$ ) before that in the coastal waters in the ECS and SCS where  $p \approx 0$  (e.g., station NSCS), while the SLA signals off the Vietnamese coast occur  $\sim 3$ – $4$  months after those in the coastal waters.

The time series of SLA and wind stress curl in Figure 6c suggest that the pumping by local wind stress curl mainly induces the SLA in the basin and east of the central Vietnam, where wind stress curl and the associated response in the current [Gan and Qu, 2008] correlate negatively with SLA. In the shallow coastal waters, the wind-forced coastal upwelling/downwelling process plays a dominant role [Gan et al., 2009a; Liu and Gan, 2014] and the effect of wind stress curl is small.

force. This pressure gradient force is much stronger in winter and may have a strong effect on the northward TWWC reported in Guan and Fang [2006].

The seasonality of the CS circulation can be better shown by conducting a harmonic analysis of sea level anomaly (SLA) amplitude ( $A$ ) and the phase lag ( $p$ ) from both observation and simulation (Figures 6a and 6b).  $p > 0$  (from January, February, March, April, May to June sequentially as  $p$  increases) and  $p < 0$  (from December, November, October, September, August to July sequentially as  $p$  decreases) represent a time lag and advance ( $\sim 1$  d/degree, relative to a reference time of 1 January when  $p = 0$ ) of the SLA seasonal variation over a period of 1 year, respectively.

Relatively strong seasonal variation of SLA is observed over the shelves shallower than 200 m. In these regions,  $A$  exceeds 0.1 m and increases shoreward. The contours of  $A$  generally follow the orientation of the isobaths over the shelf, reflecting the influence of shelf topography on the seasonal monsoonal wind-forced circulation [e.g., Gan et al., 2009a; Liu and Gan, 2014].  $A$  decreases from the continental margin toward the deep basin.

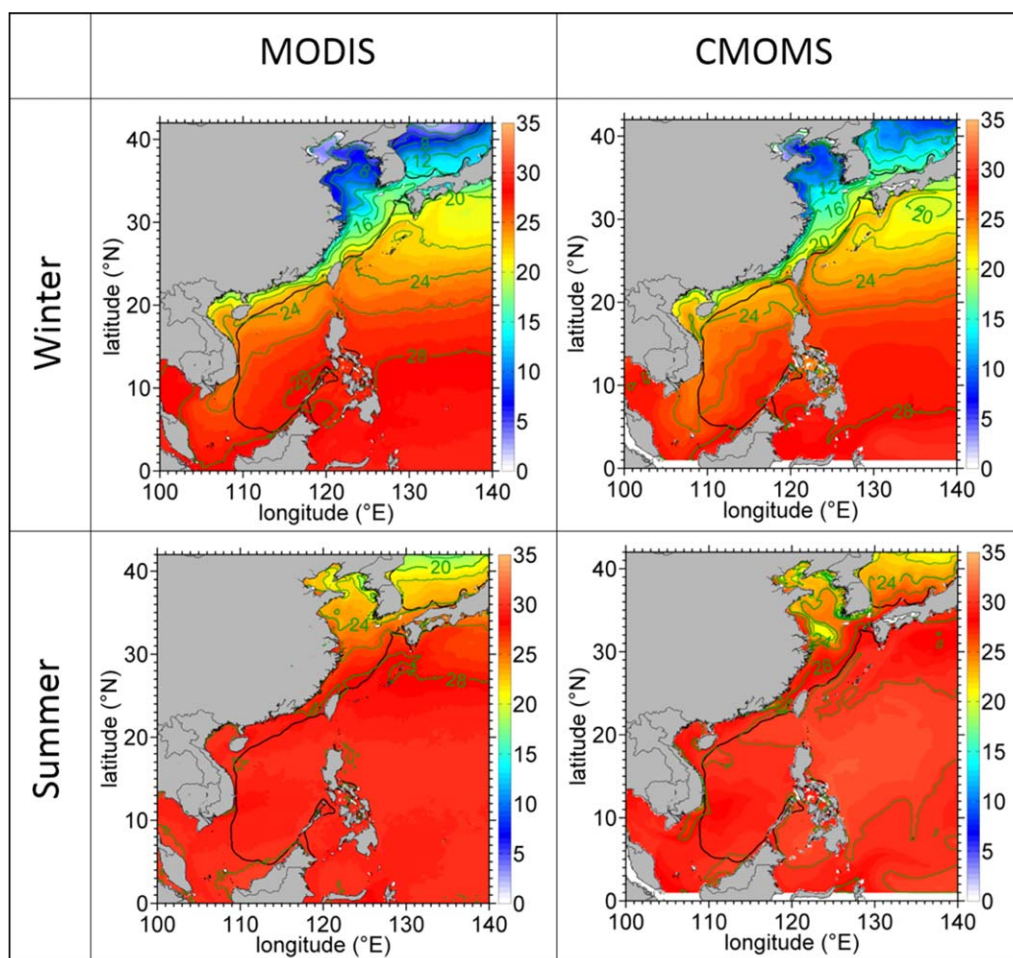


**Figure 7.** Mean sea surface temperatures (SSTs, °C) from the MODIS data (averaged from 2002 to 2013) and the model for winter and summer. The black solid line marks the 200 m isobath.

### 3.2. Hydrography and Tides

#### 3.2.1. Thermal Characteristics

The seasonal sea surface temperature (SST) distribution in Figure 7 and the time series of SSTs in the different seas obtained from CMOMS and satellite remote sensing MODIS (Moderate Resolution Imaging Spectroradiometer, averaged from 2002 to 2013) data in Figure 8a show the spatiotemporal thermal characteristics in the CS. These thermal fields reflect the interaction between atmospheric and oceanic thermal forcing, and the heat transport facilitated by the oceanic circulation.

The SST in the CS is characterized by a distinct southward gradient that is much stronger in winter. The amplitude of the seasonal SST variation increases northward and the maximum seasonal SST difference ranges from 5°C in the SCS to 20°C in the BHS (Figure 8a). The gradient and the seasonal amplitude reflect mainly the spatial variation of the air-sea heat flux in the CS.

Along the coast of the CS, heat advection driven by the strong coastal currents attenuates the meridional SST gradient. As a result, surface isotherms align with the coastline, and there is a strong cross-shelf thermal gradient along the China shelf seas in winter, which might have contributed to the northward flowing TWWC because of a thermal-wind effect.

The model satisfactorily captured the observed variable water masses in the CS. Taking the SCS as an example, the  $T$ - $S$  diagram (Figure 8b) shows that there is a large variation of the water masses as a result of the physical transport from different sources. These sources involve the land-sea interaction

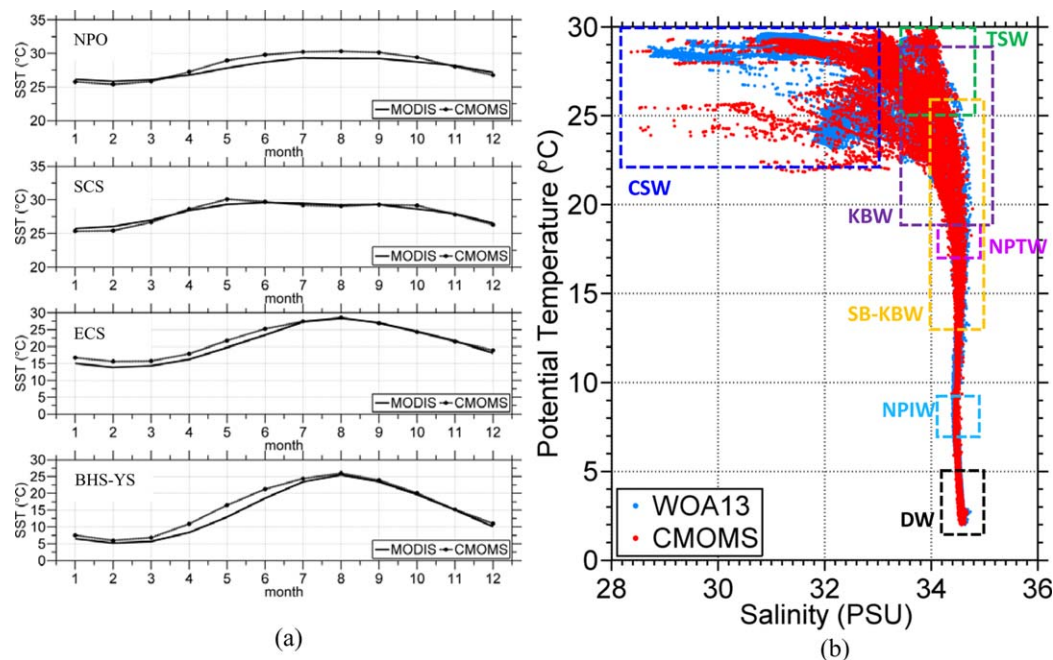


**Figure 8.** (a) Time series of SST ( $^{\circ}\text{C}$ ) from remotely sensed measurements of MODIS (solid lines, averaged from 2002 to 2013) and model results (dashed lines) in the North Pacific Ocean (NPO), SCS, ECS, and BHS-YS; (b) T-S diagram in the SCS (west of  $121^{\circ}\text{E}$ ,  $1^{\circ}\text{N}$ – $24^{\circ}\text{N}$  but excluding Sulu Sea) from WOA13 and CMOMS. The water masses in the SCS include: Continental Shelf Waters (CSW) [Rojana-Anawat *et al.*, 2000], Tropical Surface Waters (TSW) [Qu *et al.*, 1999], Kuroshio Branch Waters (KBW) [Jan *et al.*, 2006], North Pacific Tropical Waters (NPTW) [Qu *et al.*, 2000], North Pacific Intermediate Waters (NPIW) [Qu *et al.*, 2000], Subsurface Kuroshio Branch Waters (SB-KBW) [Jan *et al.*, 2006], and Deep Waters (DW) [Dippner and Loick-Wilde, 2011].

in the coastal waters and the three-dimensional water exchange between the SCS basin and the adjacent seas. The low  $S$  and high  $T$  Continental Shelf Waters result mainly from the Mekong River discharge into the Gulf of Thailand and adjacent shelves [Rojana-Anawat *et al.*, 2000] and from discharge off the Pearl River Estuary [Gan *et al.*, 2009b]. The waters with  $28^{\circ}\text{C} < T < 30^{\circ}\text{C}$  and  $S < 32$  psu are the water masses in the Gulf of Thailand. The waters with  $22^{\circ}\text{C} < T < 26^{\circ}\text{C}$  and  $S < 32$  psu, shown in the CMOMS but not in the WOA13 data, are the shelf waters near the Pearl River Estuary. The Continental Shelf Waters are generally  $\sim 10$  m thick but thicker in winter. In the basin away from the shelf region in the northern SCS, the water mass in the upper 100 m is the saltier and warmer Kuroshio Branch Waters from the Kuroshio intrusion through the LS, particularly during winter [Jan and Chao, 2003]. The southern SCS basin is occupied by warmer Tropical Surface Waters [Qu *et al.*, 1999], which originate in the northern Pacific Ocean, neighboring the intertropical convergence zone and transport into the SCS by the Kuroshio intrusion. The North Pacific Tropical Waters, situated at depths between 120 and 150 m, originate in the northern Pacific Ocean at about  $20^{\circ}\text{N}$ ,  $140^{\circ}\text{E}$ – $160^{\circ}\text{W}$  with a salinity maximum (34.75–35.25 psu) because of excessive evaporation in the upper layer of the SCS basin [Qu *et al.*, 1999]. In the subsurface layer of the northern SCS, the Subsurface Kuroshio Branch Waters occupy the depths between 100 and 200 m throughout the year [e.g., Jan *et al.*, 2006]. The North Pacific Intermediate Waters are confined to a thin layer between 480 and 500 m. These waters originate in the northern Pacific subtropical gyre and advect into the SCS through the LS [e.g., Qu *et al.*, 2000]. There is little data for the deep basin of the SCS. Following Dippner and Loick-Wilde [2011], we define the Deep Waters as having a temperature of  $\sim 2.5^{\circ}\text{C}$  and salinity of 34.6 psu. These Deep Waters form the second salinity maxima in the SCS.

### 3.2.2. Tides

Tidal mixing plays an important role in determining the hydrography and circulation, by enhancing mixing in the ocean due to internal tides and waves [e.g., Jan *et al.*, 2007]. Amplification of tidal effect occurs in the shallow shelf regions such as in the BHS, YS, and ECS.

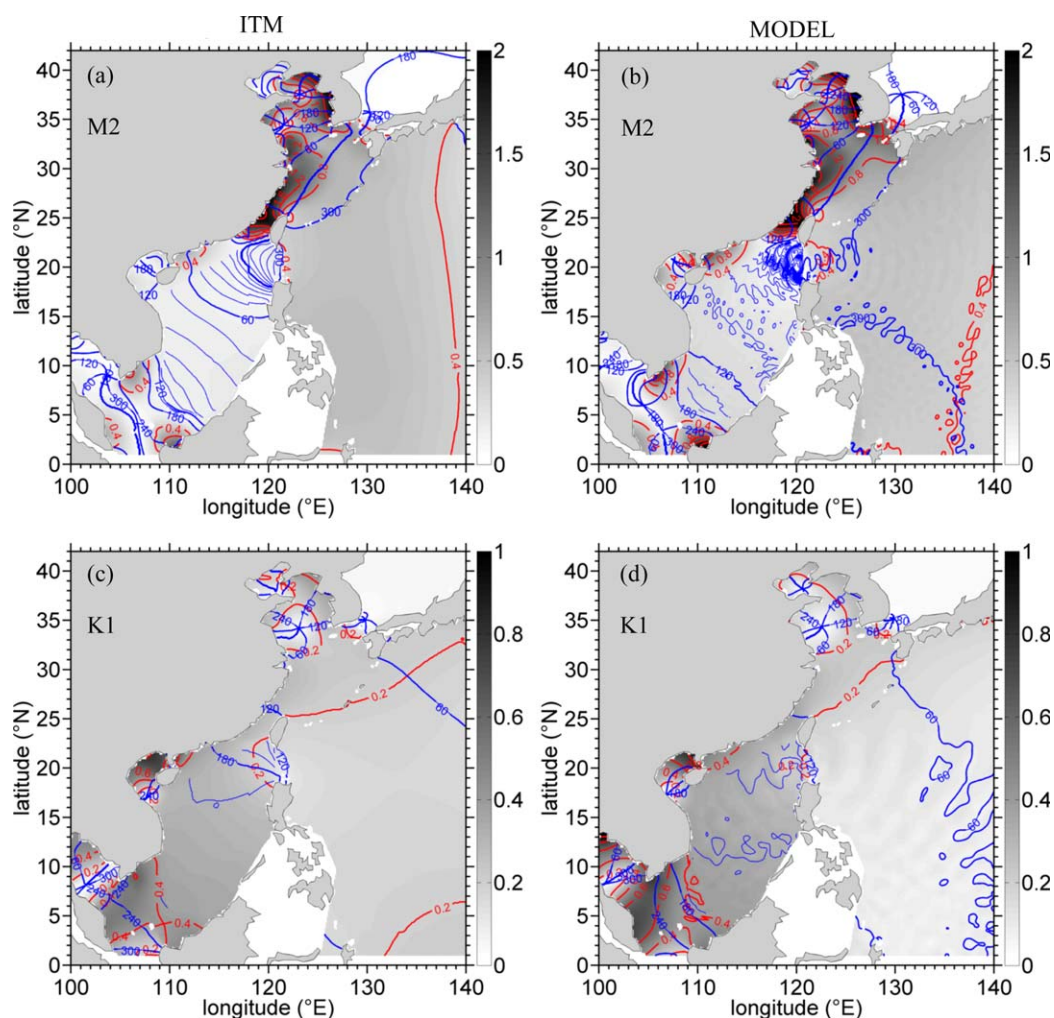


**Figure 9.** Cotidal charts of (a, b)  $M_2$  constituent and (c, d)  $K_1$  constituent from (a, c) ITM and (b, d) model, respectively. The red curves are coamplitude lines (m) and the blue curves are cophase lines ( $^\circ$ ). The gray shading represents the tidal amplitude (m).

The simulated tidal amplitudes and phases (Figure 9) agree well with those from the ITM [Egbert *et al.*, 1994]. In particular, both CMOMS and the ITM results show the resonance of  $K_1$  tide in the SCS, as in Zu *et al.* [2008], and the amplification of the  $M_2$  tide in the ECS. The results show that there are amphidromic points of the  $M_2$  and  $K_1$  tides in the YS, as in Guo and Yanagi [1998]. In contrast to the barotropic tides in the ITM, our results also demonstrate the existence of fluctuations that have a wavelength of  $\sim 100$  km in the WPO, particularly near the LS and east of Philippine Islands, similar to those identified by Niwa and Hibiya [2001]. These regions with complex bottom bathymetry have long been recognized as the typical sources of internal tide formation and are the places where the barotropic tidal energy dissipates in the stratified ocean [Jan *et al.*, 2007]. The overall effect of tidal forcing on the circulation in the CS and its hydrographic features are complex and we will study it in a separate paper.

The simulated and observed results in Figures 4–9 are reasonably consistent. Together with the consistency between the model and observations of the circulation fields that will be described later, the results suggest that the model is able to realistically capture the circulation and forcing conditions in the CS, which establishes a level of confidence in the dynamic and thermodynamic capability of the model.

#### 4. Vertically Varied Circulation

The circulations vary greatly across the individual seas of the CS, at different depths of the water column and during different seasons. In addition to monsoonal wind forcing, time-dependent and spatially variable

lateral flows into and out of the CS through the straits (or the continental slope in case of the ECS) shape the three-dimensional circulation and transport in the CS.

#### 4.1. Layered Circulation

The time-dependent, three-dimensional circulation in the CS is seen in the seasonal layer-integrated stream function ( $\psi$ ) in the upper, middle, and deep layers in Figure 10. The corresponding relative vorticity in the upper ocean is shown in Figure 11 and the time series of depth-dependent horizontally averaged vorticity in the individual seas is shown in Figure 12. By inspecting the results in Figure 12, we selected three layers in the SCS with water depths  $h < 750$ ,  $750\text{--}1500$ , and  $>1500$  m for Figure 10.

##### 4.1.1. Upper Layer (0–750 m)

In the WPO, the NEC and the Kuroshio, which are the major currents adjacent to the CS, exhibit a strong seasonality, as indicated by  $\psi$  in Figure 10. In winter, a weakened NEC bifurcates at the farther northern latitude than that in summer. This bifurcation, in turn, weakens the Kuroshio and enhances the westward intrusion of the Kuroshio into the SCS through the LS in winter [e.g., Qu *et al.*, 2000; Gan *et al.*, 2006]. This seasonal variation of the Kuroshio's intensity is also shown in Figure 11 by the vorticity gradient across the flow east of the LS and off the ECS, and by the corresponding ADT in Figure 4.

Over the ECS shelf, negative cross-shelf gradient of  $\frac{\partial\psi}{\partial x^*}$ , where  $x^*$  is a cross-shelf seaward coordinate, represents the alongshore shelf transport. Relatively strong transport occurs in the TWS and in the Tsushima Strait. There exists a net northward transport over the ECS, similar to that observed by Guan and Fang [2006]. The negative and positive vorticity bands near the coast south of the Changjiang Estuary (Figure 11) indicate that there is a wind-driven and buoyancy-driven (from Changjiang River discharge) southward jet. This jet extends along the entire coast in winter, but is mainly restricted to the region near the estuary in summer. The vorticity bands over the mid-ECS shelf reflect the cross-shelf variation of wind-driven along shelf current.

In the SCS during winter, the circulation in the upper layer is cyclonic and spans the entire basin with a stronger intensity in the northern part of the SCS basin (Figure 10). This circulation trait results from the forcing of the northeasterly monsoon wind stress, positive wind stress curl (Figure 3), and stronger winter Kuroshio intrusion along the continental slope around the SCS (also see Section 5) [e.g., Qu, 2000; Gan *et al.*, 2006]. During summer, a southwestward current along the northern slope and an eastward returning current at  $\sim 13^\circ\text{N}$  form a cyclonic circulation in the northern part of the basin and a weak anticyclonic circulation in the southern part of the basin. The basin dipole wind stress curl (Figure 3) and the recirculation of a coastal jet separation to the east of Vietnam [Gan and Qu, 2008] jointly govern the circulation in summer.

The half-basin circulation pattern in both seasons produces a larger transport exiting the SCS through the Mindoro Strait than through the Karimata Strait and TWS (also see section 5). This indicates that the LS inflow exits the SCS mainly via the Mindoro Strait, the main pathway of the South China Sea throughflow (SCSTF) [Qu *et al.*, 2006].

##### 4.1.2. Middle Layer (750–1500 m)

In the middle layer, the current in the WPO is generally weak and the signature of the Kuroshio shows only in the anticyclonic recirculation off the southern Japan (Figure 10). During both seasons, the circulation in the middle layer of the SCS is anticyclonic, although not as circular as that in the upper layer. The seasonality of circulation is also much weaker than that in the upper layer.

##### 4.1.3. Deep Layer (>1500 m)

In the deep layer, a cyclonic circulation prevails in the SCS during both winter and summer, as Lan *et al.* [2013] have also found. The cyclonic circulation is present in the layer, in spite of the existence of a weak anticyclonic circulation in the deepest central basin during winter. The cyclonic circulation is stronger in summer than in winter, unlike in the upper layer where it is stronger in winter. The seasonality correlates well with the time of the deep intrusion through the LS (see section 5).

#### 4.2. Rotating Circulation

The seasonal variation of three-dimensional circulation ( $C$ ) in the individual seas of the CS is further demonstrated by the time series of domain-averaged vorticity in the water column (Figures 12a–12c). According to Stoke's theorem,

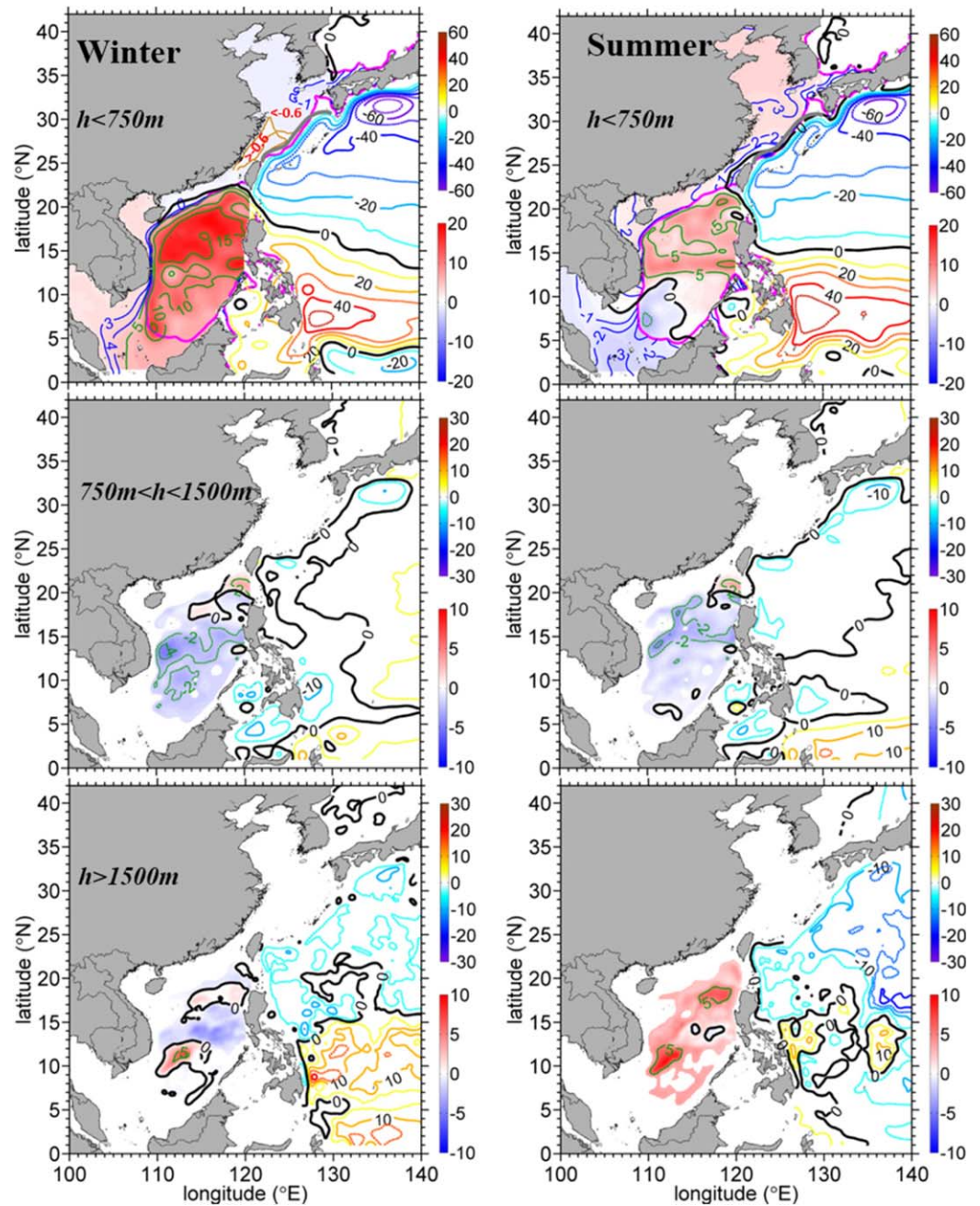


**Figure 10.** Transport (Sv) stream function in the upper layer (<750 m), middle layer (750–1500 m), and deep layer (>1500 m) in the (left column) winter and (right column) summer, respectively. The upper and lower scale bars are for the western Pacific (east of the 200 m isobath) and the CS (with different contour intervals and background color contours), respectively. The pink line in the upper layer is the 200 m isobath and grey line to the east of the ECS is the shore-side boundary of Kuroshio.

$$C = \oint \vec{V} \cdot d\vec{l} = \iint_S \zeta dS, \quad (1)$$

where  $\vec{V}$  is the velocity vector,  $\zeta$  is the relative vertical vorticity normal to  $S$ , which is the area of a specific sea for  $C$ . We exclude the shelf at  $h < 100$  m in the SCS to rule out the influence of shelf circulation [Gan *et al.*, 2009a], and at  $h > 100$  m in the ECS to rule out the influence of the Kuroshio [Liu and Gan, 2012]. The areas of the SCS, ECS, and YS are defined in Figure 12d. Results from equation (1) in Figure 12 represent the circulation pattern in the specific sea of the CS. Figure 13 illustrates the rotating currents by vorticity and

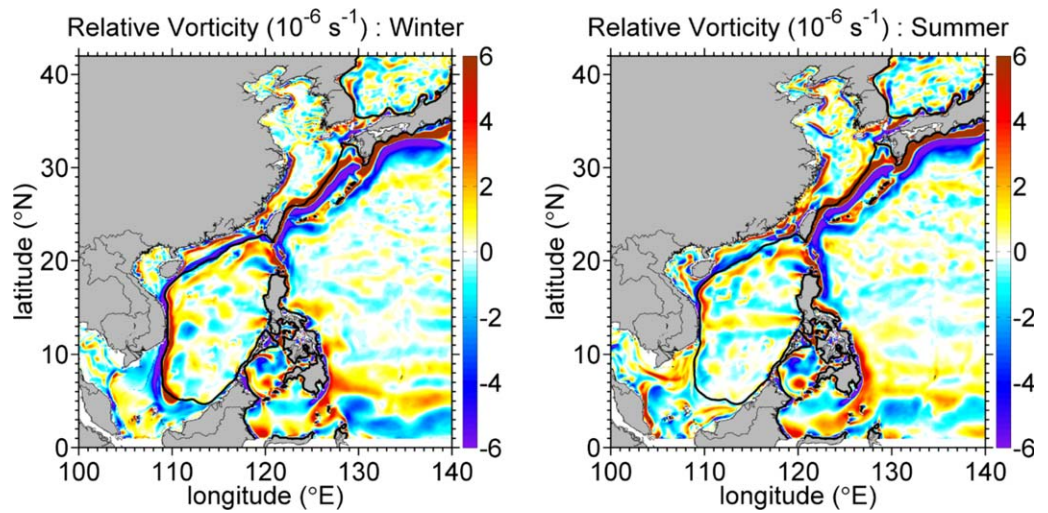


**Figure 11.** Relative vorticity ( $10^{-6} \text{ s}^{-1}$ ) in the upper 750 m in the CS during winter and summer. The black solid line indicates the 200 m isobath.

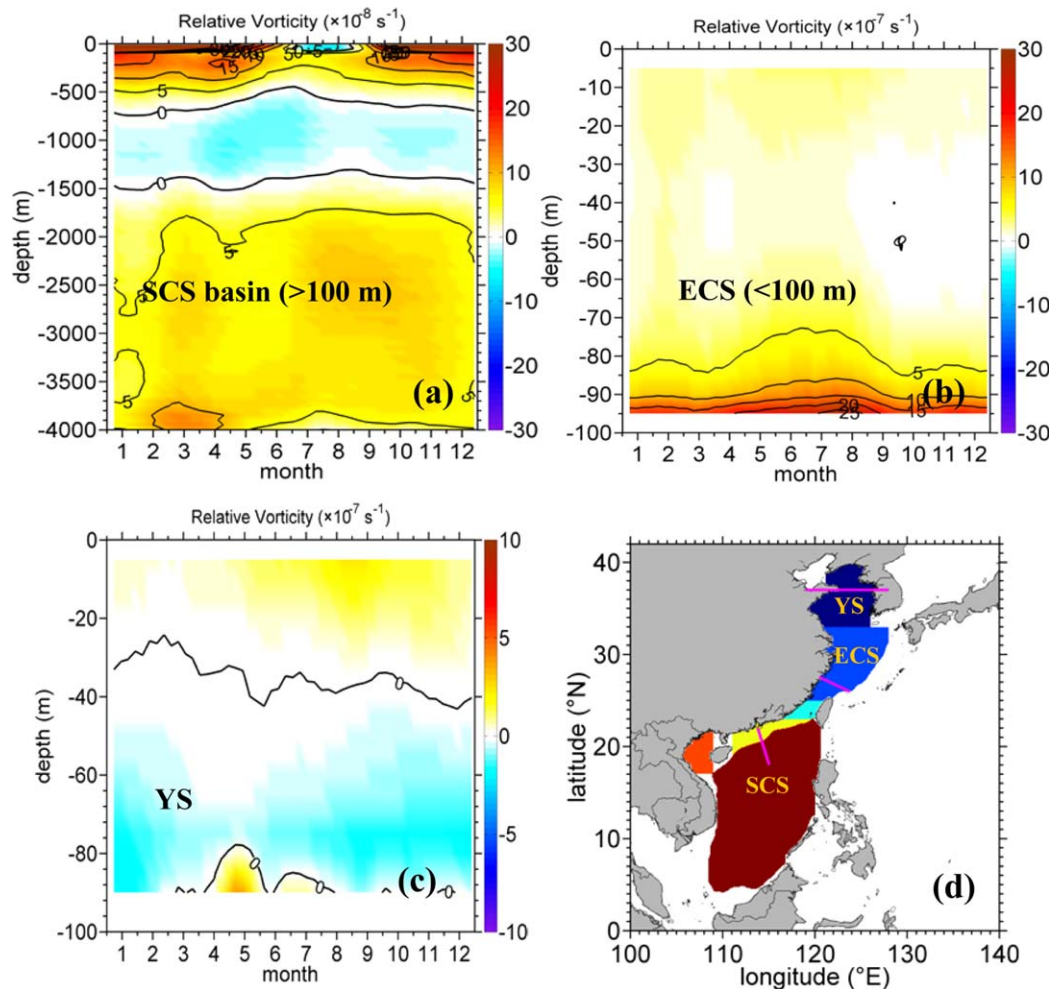


**Figure 12.** Time series of domain-averaged depth-dependent relative vorticity in (a) the SCS basin ( $h > 100 \text{ m}$ ), (b) the ECS ( $h < 100 \text{ m}$  excluding TWS), (c) the YS, and (d) the domains for each of the seas. The pink lines are three transects in the SCS, ECS, and YS.

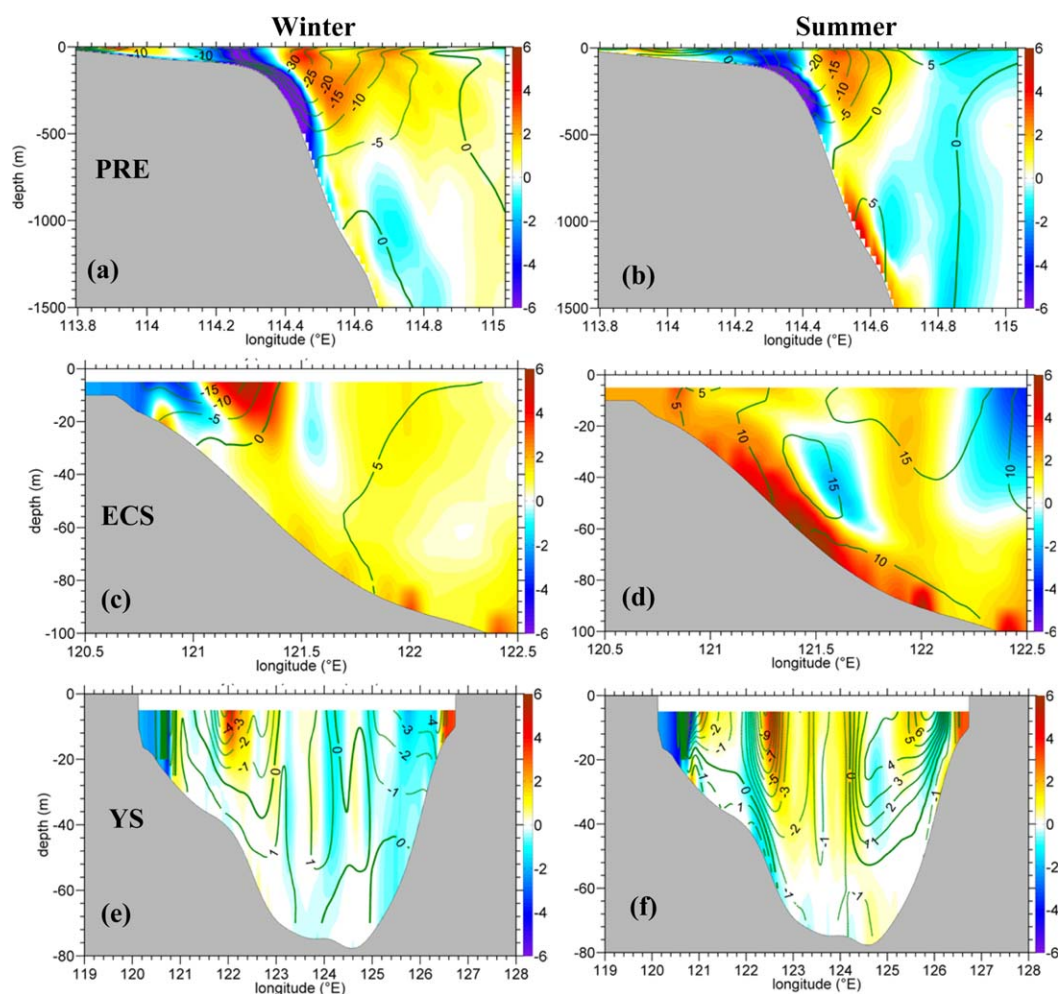


**Figure 13.** Cross sections of vertical vorticity ( $10^{-6} \text{ s}^{-1}$ ; color contours) and velocity ( $\text{cm s}^{-1}$ ; contour lines) normal to the transects along the (a, b) PRE line, (c, d) ECS line, and (e, f) YS line along  $36^\circ\text{N}$  in (left column) winter and (right column) summer. The positive velocities are directed eastward, northward, and northward in the PRE, ECS, and YS lines, respectively. The locations of the PRE, ECS, and YS lines are marked in Figure 12.

the slope/shelf currents normal to the cross-shelf transects across the Pearl River Estuary (PRE), ECS, and YS lines in the respective seas.

#### 4.2.1. South China Sea Basin

The time series of domain-averaged vorticity in the water column presents clearly a three-layer alternating cyclonical-anticyclonical-cyclonical circulation (CACC) in the upper-middle-lower layers of the water column in the SCS (Figure 12a). This result further illustrates the nature of the seasonal circulation shown in Figure 10.

In the upper layer, vorticity input from the wind stress curl (Figure 3) and positive horizontal shear vorticity on the seaside of the slope current (Figures 11 and 13a and 13b) jointly form the cyclonic circulation (Figure 12a). The slope current and thus the basin circulation are much stronger in winter (Figures 13a and 13b). As a result, a thicker (thinner) upper layer occurs in winter (summer) partly because of the conservation of potential vorticity in the first order.

In the middle layer, the basin circulation is anticyclonic for the entire year, but is relatively strong in late spring and early summer (Figure 12a). There exists a very weak current in the northern slope below the upper layer in winter (Figure 13a). This current, however, reverses direction between 1000 and 1500 m and strengthens in summer when the slope current in the upper layer weakens. The prevailing outflow in this layer of the LS (see section 5) attributes largely to the middle layer anticyclonic circulation.

In the deep layer, the basin-averaged circulation is cyclonic (Figure 12a). The deep layer circulation strengthens from July to early fall. In general, a relatively strong circulation occupies the depths between 2000 and 3000 m.

The three-layer CACC structure and its dynamics control in the SCS were recently reported by Gan *et al.* [2016]. Besides the vorticity imparted by wind stress curl, their analyses of vorticity balance suggested that the input of planetary vorticity flux by the inflow-outflow-inflow in the LS, after being offset by the vorticity induced by the interaction between baroclinic flow and basin topography or the Joint Effect of Baroclinicity and Bottom Relief (JEBAR), formed the three-layer CACC.

#### 4.2.2. East China Sea Shelf

In the ECS shelf, positive vorticity prevails in the entire water column throughout the year (Figure 12b). The magnitude of this positive vorticity decreases from the upper layer (<30 m) to the middle layer (30–70 m) in the ECS, but it intensifies in the bottom layer (70–100 m) of the deep offshore waters. *In winter*, the wind and buoyancy forcing from the Changjiang River discharge induces the southward ECS coastal jet (Figure 13c). The jet forms a strong horizontal shear in the coastal waters. This coastal jet weakens seaward and it encounters the northward TWWC at the water depth of ~40 m (Figure 13c). Thus, we attribute the presence of the positive vorticity in winter mainly to the positive shear vorticity seaside of the southward jet and to the shearing flow between the jet and northward TWWC.

*In summer*, the shear vorticity, which arises from the shoreward decrease in the northward wind-driven alongshore velocity, contributes to the positive vorticity (Figure 13d). The northward shelf current has a multicore structure, which is induced by the variable slope of shelf topography [Liu and Gan, 2014, 2015]. The multicore shelf current leads to variable, but mainly positive vorticities between the no-slip coast and jet, and between the jets themselves. The prevailing positive wind stress curl in summer (Figure 3) also contributes to the cyclonic circulation in summer, even though the curl is relatively weak.

Overall, the shelf current over the ECS flows cyclonically due to the cross-shelf variation of the along-shelf current. In the middle layer, the weaker alongshore current and the velocity shear, and the formation of negative vorticity due to horizontal variable current form the relatively weak positive vorticity (Figures 13c and 13d). On the other hand, the shore-side shear in the Kuroshio contributes to the larger positive vorticity in the deep layer.

#### 4.2.3. Yellow Sea

The mean circulations in the upper (<~40 m) and lower layers (>~40 m) of the YS are cyclonic and anticyclonic, respectively (Figure 12c). *In winter*, the northward intrusive Yellow Sea Warm Current (YSWC) [e.g., Isobe, 2008] flows along the central topographic trough (Figure 13e). The shears in YSWC and in a southward returning Yellow Sea Coastal Current (YSCC) at a water depth of ~40 m along the west coast generate the cyclonic circulation in the western YS. Likewise, the YSWC and a southward current along the deep eastern coast (or West Korea Current; WKC) yield the anticyclonic circulation in the eastern YS. Naimie *et al.* [2001] also observed the same circulation pattern in the YS. The cyclonic circulation in the western YS is stronger than the anticyclonic one in the eastern YS, which produces a weak cyclonic average circulation in the YS. In the lower layer during winter, the YSCC is weak and the shears in the intrusive YSWC and WKC generate the anticyclonic deep circulation.

*In summer*, a northward WKC and a southward YSCC (Figure 13f) form the stronger cyclonic circulation in the upper layer (Figure 12c). The offshore weakening of the strong southward YSCC or positive shear vorticity contributes largely to the cyclonic circulation in the upper layer. We attribute the negative vorticity in the lower layer mainly to the velocity shear between the YSCC and the coast.

These results suggest that the seasonal circulation in the YS is jointly forced by intrusion of the external current and the monsoonal wind-forced coastal currents. It is worth noting that, according to our numerical experiment, the tidal forcing plays an important role in shaping the YS circulation.

The results in Figures 12 and 13 illustrate the overall rotating circulation patterns and the spatiotemporal characteristics of the currents associated with these patterns in the SCS, ECS and YS.

## 5. Forced by Exchanging Flows With Adjacent Seas

The forcing by the time-dependent, three-dimensional water exchanges between the CS and the adjacent oceans shapes critically the circulation characteristics described in the previous sections, in addition to the

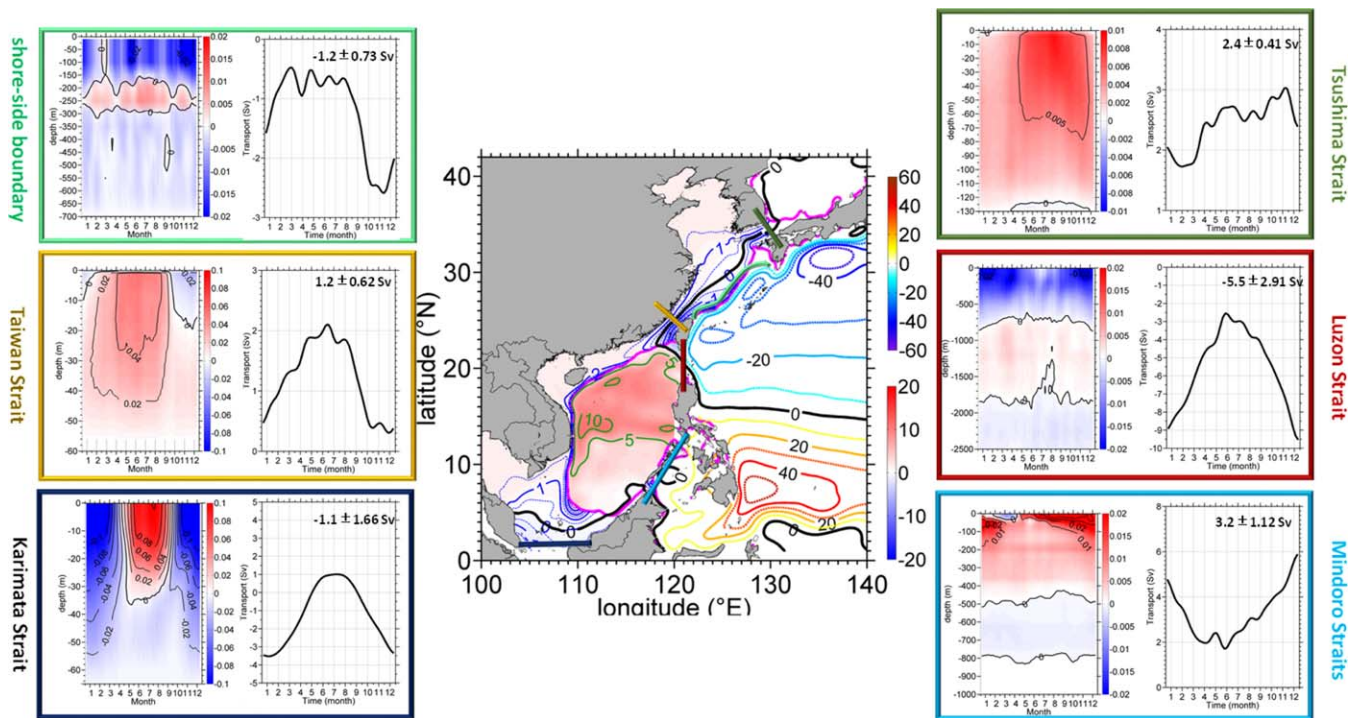


**Figure 14.** Time series of depth-integrated transport (Sv) and depth-dependent mass flux ( $10^6 \text{ m}^2 \text{ s}^{-1}$ ) through the straits around the CS and across the shore-side boundary (SSB, light green line) of the Kuroshio in the ECS. Each strait/SSB is indicated by a specific color bar and the result for each strait is shown in a box of the corresponding color. The background contours in the CS domain represent the annual mean transport stream function in the upper 750 m. The positive value refers to northward flows in the Taiwan, Karimata, and Tsushima Straits, outflows in the Luzon and Mindoro Straits, and seaward flow along the SSB. The pink line represents the 200 m isobath.

monsoonal wind forcing. Currently we are still largely uncertain about the transport magnitudes and phases of the inflows/outflows in these exchanges. We also do not know how these inflows/outflows are spatio-temporally linked with each other and with the circulation in the CS. In fact, the uncertainties about these exchanges often have led to different interpretations and speculations of the circulation and the forcing process in the CS. We present the time-dependent, three-dimensional water exchanges between the CS and adjacent seas in Figure 14, and discuss strong coherences among these exchanges and between the exchanges with the circulation characteristics in the CS.

The transports for the water exchange between the CS and adjacent seas and their coherences can be described as follows. A  $\sim -5.5$  Sv (annually and water-column-integrated transport) westward transport intrudes into the SCS basin through the LS from the WPO. Conveyed by the slope in the SCS, a  $\sim 1.2$  Sv of the intrusive transport exits the basin through the TWS in the north, and a  $\sim 1.16$  Sv exits through the Karimata Strait and a  $\sim 3.2$  Sv through the Mindoro Strait in the south. In the YS and ECS, a  $\sim -1.2$  Sv shoreward transport across the slope off the ECS and a  $\sim 1.2$  Sv northward transport in the TWS form a  $\sim 2.4$  Sv northward transport through the Tsushima Strait. Obviously, the total transports in these exchange flows are constrained by the mass balances in each individual sea, and in the entire CS as well. These linked transports interact with the wind-forced currents and shape the CS circulation.

The exchanging flows show strong seasonality around the periphery of the CS. In the SCS, the transports in the four straits exhibit concurrently a strong annual U-shaped (or inverted U-shaped) temporal variation, with weaker inflows/outflows in summer and stronger ones during the other seasons. We associate the U-shaped variation of the transports predominantly with the variable strength of the Kuroshio separation at the entrance of the LS extrinsically [e.g., Qu, 2000; Gan et al., 2006; Wu and Hsin, 2012; Hsin et al., 2012] and with the interaction between the transports and the SCS circulation intrinsically [Gan et al., 2016].

Unlike the annual U-shaped temporal variation in the South China Sea and in the TWS, the transports in shoreward intrusion along the SSB of Kuroshio and Tsushima Strait have distinct semiannual variation and they reach the largest and smallest values in late fall and early spring, respectively. They are relatively strong

in the second half of the year. This semiannual variation reflects the combined effect of the seasonal variations of transports crossing the TWS and the SSB of the Kuroshio. The northward transport in the TWS during winter mainly occurs in the deep waters east of the strait due to the northward Kuroshio intrusion. However, the TWS transport during summer is primarily driven by the southwesterly wind.

The transports that cross the straits and the slope are vertically variable. The transports in the deeper layer are much weaker than the ones in the upper layer. In the LS, the prominent sandwich structure of inflow-outflow-inflow is evident in the upper-middle-lower layers. Although the complete mechanism governing the three-layer structure is still unclear, it is conceivable that this sandwich structure is responsible for the alternating three-layer CACC spinning circulation in the SCS (Figures 10 and 12). We estimate that the transports in the upper, middle, and lower layers of the LS are  $\sim -5.9$ , 1.4, and  $-0.9$  Sv. A  $\sim 3.2$  Sv outward transport in the Mindoro Strait mainly occurs in the upper 400 m while there is a weak inflow of  $\sim 0.1$  Sv in the deep channels southwest of the main Mindoro Strait channel. Because the inflow from the LS is in the upper and lower layers of the SCS basin, we expect that a downward mass flux from the upper layer and an upward mass flux from the deep layer compensate for the outflow in the middle layer of the LS. Thus, in the domain-averaged scale, little of the deep intrusive water would have reached the upper layer, although the strong upward motions might have occurred in isolated locations in the SCS, subject to the influence of local topography, eddy, waves, and other local processes. We believe that the deep transport, such as the one in the LS, plays an important role in maintaining the three-dimensional SCS circulation.

The shoreward transport crossing the SSB of the Kuroshio off the ECS (light green line in Figure 14) is mainly found in the upper ( $\sim 1.0$  Sv) and lower ( $\sim 0.7$  Sv) layers, which accounts for the portions of the Kuroshio intrusion in the ECS (west of  $127^\circ\text{E}$ ) and the deep channel to the southwest of Japan, respectively. The ECS portion is mainly observed off the northeast coast of Taiwan and in the central ECS. The net seaward transport at a depth of  $\sim 250$  m along the SSB in Figure 14 accounts for the outflow southwest of Japan as the Kuroshio loops around the region.

## 6. Summary and Conclusion

Ocean circulation in the CS is intrinsically driven by seasonal monsoonal winds over the linked shelf and basin topography, and extrinsically driven by the flow exchange through the straits and over the continental slope that borders the eastern CS. The transports of these exchange flow are coherently linked, because of the constraint of the total mass conservation in the CS. Meanwhile, the transports also interact with the intrinsic circulation to characterize the CS circulation. Among the seas that make up the CS, the circulations in the SCS and ECS are linked by the transport through the TWS. There are very few studies that coherently link different forcing processes with the circulations in the CS. As a result, our understanding of the overall CS circulation is piecewise and builds on the knowledge of the circulation in each isolated sea.

Based on observational evidence and synthesized results from previous studies in the CS, we developed a three-dimensional model to investigate the circulations in the CS in response to intrinsic and extrinsic forcings. This new CS circulation model considers regional ocean circulation dynamics and adopts a physically sensible computational domain. The model also considers regionally validated mechanical and thermodynamic forcings from atmospheric and lateral fluxes and from tides. Furthermore, the model uses numerically and physically adaptable OBCs and subscale parameterization to the CS. The model is comprehensively validated by measurements, synthesized results derived from previous studies and more importantly by scientific reasoning of the coherent circulation in the CS.

The seasonal circulation in the upper layer of the CS varies with the East Asian monsoonal winds and variation in the exchange flows. In the upper layer of the SCS, circulation is cyclonic during winter. This cyclonic circulation remains in the northern half of the SCS basin during summer while anticyclonic circulation occupies the southern half of the basin. The shelf circulation in the ECS is characterized by the northeastward and southwestward currents in summer and winter, respectively. Throughout the year, the circulation is bounded by a strong coastal current inshore and by the northward flowing Kuroshio offshore. The circulation in the YS is regulated by seasonally reversing coastal currents in the western and eastern coasts, and by variable northward intrusive current along the central topographic trough of the basin.

The circulation varies more dramatically in the shelf regions (water depth < 200 m) of the CS as a result of seasonally reversing shelf current. We attribute the circulation variability over the shelf mainly to the monsoonal wind-driven Ekman transport and that in the SCS basin to local wind stress curl pumping and the current separation along the west coast.

As a result of the time-dependent, three-dimensional circulation and the atmospheric heat fluxes, the thermal field in the upper ocean of the CS exhibits a strong seasonality. The meridional thermal gradient is strongest in winter and increases northward in the CS. A variety of water masses are observed in the SCS and their origins are related to terrestrial input, local waters and waters from adjacent open oceans.

The circulation in the CS is three dimensional and varies vertically. We found a three-layer CACC in the SCS, a cyclonically rotating flow in the entire water column of the ECS, and cyclonic and anticyclonic circulation patterns in the upper and lower layers of the YS, respectively. These rotating layered circulations prevail throughout the year, but their intensities vary seasonally. The three-layer CACC in the SCS is linked to the inflow-outflow-inflow of the three-layer transport in the LS. The horizontal variation of the shelf flow is responsible for the cyclonically rotating flow in the ECS. The seasonally and vertically variable intrusive current at the central trough, and the coastal currents to its west and east, shape the two-layer circulation in the YS. These time-dependent, three-dimensional circulations in the CS are comprehensively demonstrated in the spatiotemporal fields of velocity, ADT, the transport stream function and vorticity fields.

Circulation in the CS is closely linked with external transports. These transports interact with interior circulation in the CS and vary coherently with the overall circulation. In the SCS, the inflow in the LS mainly exits as outflow in the Mindoro Strait, following the main route of the SCSTF. The outflow in the LS associated with the anticyclonic circulation in the middle layer of the SCS basin is the major exporting conduit of the SCS water to the adjacent WPO. The prevailing net northward transport in the TWS throughout the year connects the circulations in the SCS and the ECS, and it interacts with the Kuroshio shoreward transport and the Tsushima Strait transport, and with the monsoonal wind-forced shelf current. Together they shape the seasonal shelf circulation in the ECS.

Based on a newly developed ocean circulation model, this study delineated the key kinematic characteristics of the CS circulation. Our results of transports, flow exchanges, and general circulation jointly depict that these characteristics are coherently related to the intrinsic circulation of the wind-forced current over the unique shelf and basin topography of the CS and to the extrinsic forcing of the inflow/outflow across the straits and slope around the periphery of the CS. The underlying dynamics associated with these interactively intrinsic and extrinsic forcing processes in the CS circulation will be presented in our companion paper.

#### Acknowledgments

This research was supported by the National (China) Key Basic Research Development Program (2015CB954004), the Key Project of the National Science Foundation of China (91328202), and the Hong Kong Research Grants Council (GRF16202514). The authors are grateful to Anson Cheung, Xiaozheng Zhao, and Hiusuet Kung for processing the data and to two anonymous reviewers for their useful comments and suggestions. The data for this study are available from the corresponding author at e-mail address: magan@ust.hk.

#### References

- Dai, A., and K. E. Trenberth (2002), Estimates of freshwater discharge from continents: Latitudinal and seasonal variations, *J. Hydrometeorol.*, 3(6), 660–687.
- Dippner, J. W., and N. Loick-Wilde (2011), A redefinition of water masses in the Vietnamese upwelling area, *J. Mar. Syst.*, 84, 42–47.
- Egbert, G. D., A. F. Bennett, and M. G. G. Foreman (1994), TOPEX/Poseidon tides estimated using a global inverse model, *J. Geophys. Res.*, 99, 24,821–24,852.
- Fairall, C. W., E. F. Bradley, J. E. Hare, A. A. Grachev, and J. B. Edson (2003), Bulk parameterization of air-sea fluxes: Updates and verification for the COARE algorithm, *J. Clim.*, 16(4), 571–591.
- Fang, G. H., B. Zhao, and Y. Zhu (1991), Water volume transport through the Taiwan Strait and the continental shelf of the East China Sea measured with current meters, in *Oceanography of Asian Marginal Seas*, edited by K. Takano, pp. 345–358, Elsevier.
- Fang, G. H., R. D. Susanto, S. Wirasantosa, F. Qiao, A. Supangat, B. Fan, Z. Wei, B. Sulistiyo, and S. Li (2010), Volume, heat, and freshwater transports from the South China Sea to Indonesian seas in the boreal winter of 2007–2008, *J. Geophys. Res.*, 115, C12020, doi:10.1029/2010JC006225.
- Flather, R. A. (1976), A tidal model of the northwest European continental shelf, *Mem. Soc. R. Sci. Liege*, 10, 141–164.
- Gan, J., and J. S. Allen (2005), On open boundary conditions for a limited-area coastal model off Oregon. Part 1: Response to idealized wind forcing, *Ocean Modell.*, 8, 115–133.
- Gan, J., and T. Qu (2008), Coastal jet separation and associated flow variability in the southwest South China Sea, *Deep Sea Res., Part I*, 55, 1–19, doi:10.1016/j.dsr.2007.09.008.
- Gan, J., L. Mysak, and D. Straub (1998), Simulation of the South Atlantic Ocean circulation and its seasonal variability, *J. Geophys. Res.*, 103, 10,241–10,251.
- Gan, J., H. Li, E. N. Curchitser, and D. B. Haidvogel (2006), Modeling South China Sea circulation: Response to seasonal forcing regimes, *J. Geophys. Res.*, 111, C06034, doi:10.1029/2005JC003298.
- Gan, J., Y. Y. Cheung, X. G. Guo, and L. Li (2009a), Intensified upwelling over a widened shelf in the northeastern South China Sea, *J. Geophys. Res.*, 114, C09019, doi:10.1029/2007JC004660.
- Gan, J., L. Li, D. Wang, and X. Guo (2009b), Interaction of river plume with coastal upwelling circulation in the northeastern South China Sea, *Continental Shelf Res.*, 29, 728–740, doi:10.1016/j.csr.2008.12.002.

- Gan, J., H. Ho, and L. Liang (2012), Dynamics of intensified downwelling circulation over a widened shelf in the northeastern South China Sea, *J. Phys. Oceanogr.*, *43*(1), 80–94, doi:10.1175/JPO-D-12-02.1.
- Gan, J., Z. Liu, and C. Hui (2016), A three-layer alternating spinning circulation in the South China Sea, *J. Phys. Oceanogr.*, doi:10.1175/JPO-D-16-0044.1.
- Guan, B. X., and G. H. Fang (2006), Winter counter-wind currents off the southeastern China coast: A review, *J. Oceanogr.*, *62*(1), 1–24, doi:10.1007/s10872-006-0028-8.
- Guo, X., and T. Yanagi (1998), Three-dimensional structure of tidal current in the East China Sea and the Yellow Sea, *J. Oceanogr.*, *54*, 651–668.
- Guo, X., Y. Miyazawa, and T. Yamagata (2006), The Kuroshio onshore intrusion along the shelf break of the East China Sea: The origin of the Tsushima Warm Current, *J. Phys. Oceanogr.*, *36*(12), 2205–2231, doi:10.1175/JPO2976.1.
- Hsin, Y.-C., C.-R. Wu, and S.-Y. Chao (2012), An updated examination of the Luzon Strait transport, *J. Geophys. Res.*, *117*, C03002, doi:10.1029/2011JC007714.
- Isobe, A. (2008), Recent advances in ocean-circulation research on the Yellow Sea and East China Sea shelves, *J. Oceanogr.*, *64*(4), 569–584, doi:10.1007/s10872-008-0048-7.
- Jan, S., and S. Y. Chao (2003), Seasonal variation of volume transport in the major inflow region of the Taiwan Strait: The Penghu Channel, *Deep Sea Res., Part II*, *50*(6–7), 1117–1126.
- Jan, S., D. D. Sheu, and H.-M. Kuo (2006), Water mass and throughflow transport variability in the Taiwan Strait, *J. Geophys. Res.*, *111*, C12012, doi:10.1029/2006JC003656.
- Jan, S., C.-S. Chern, J. Wang, and S.-Y. Chao (2007), Generation of diurnal K1 internal tide in the Luzon Strait and its influence on surface tide in the South China Sea, *J. Geophys. Res.*, *112*, C06019, doi:10.1029/2006JC004003.
- Jan, S., Y. J. Yang, J. Wang, V. Mensah, T.-H. Kuo, M.-D. Chiou, C.-S. Chern, M.-H. Chang, and H. Chien (2015), Large variability of the Kuroshio at 23.75°N east of Taiwan, *J. Geophys. Res. Oceans*, *120*, 1825–1840, doi:10.1002/2014JC010614.
- Lan, J., N. Zhang, and Y. Wang (2013), On the dynamics of the South China Sea deep circulation, *J. Geophys. Res. Oceans*, *118*, 1206–1210, doi:10.1002/jgrc.20104.
- Lien, R.-C., B. Ma, Y.-H. Cheng, C.-R. Ho, B. Qiu, C. M. Lee, and M.-H. Chang (2014), Modulation of Kuroshio transport by mesoscale eddies at the Luzon Strait entrance, *J. Geophys. Res. Oceans*, *119*, 2129–2142, doi:10.1002/2013JC009548.
- Liu, Z., and J. Gan (2012), Variability of the Kuroshio in the East China Sea derived from satellite altimetry data, *Deep Sea Res., Part I*, *59*, 25–36.
- Liu, Z., and J. Gan (2014), Modeling study of variable upwelling circulation in the East China Sea: Response to a coastal promontory, *J. Phys. Oceanogr.*, *44*, 1078–1094, doi:10.1175/JPO-D-13-0170.
- Liu, Z., and J. Gan (2015), Upwelling induced by the frictional stress curl and vertical squeezing of the vortex tube over a submerged valley in the East China Sea, *J. Geophys. Res. Oceans*, *120*, 2571–2587, doi:10.1002/2015JC010715.
- Mellor, G. L., and T. Yamada (1982), Development of a turbulence closure model for geophysical fluid problems, *Rev. Geophys.*, *20*, 851–875.
- Naimie, E. C., C. A. Blain, and D. R. Lynch (2001), Seasonal mean circulation in the Yellow Sea—a model-generated climatology, *Deep Sea Res., Part I*, *21*, 667–695.
- Niwa, Y., and T. Hibiya (2001), Numerical study of the spatial distribution of the M2 internal tide in the Pacific Ocean, *J. Geophys. Res.*, *106*, 22,441–22,449.
- Qiu, B., and R. Lukas (1996), Seasonal and interannual variability of the North Equatorial Current, the Mindanao Current, and the Kuroshio along the Pacific western boundary, *J. Geophys. Res.*, *101*, 12,315–12,330.
- Qiu, Y., L. Li, C.-T. Chen, X. Guo, and C. Jing (2011), Currents in the Taiwan Strait as observed by surface drifters, *J. Oceanogr.*, *67*(4), 395–404, doi:10.1007/s10872-011-0033-4.
- Qu, T. (2000), Upper-layer circulation in the South China Sea, *J. Phys. Oceanogr.*, *30*(6), 1450–1460.
- Qu, T., and Y. T. Song (2009), Mindoro Strait and Sibutu Passage transports estimated from satellite data, *Geophys. Res. Lett.*, *36*, L09601, doi:10.1029/2009GL037314.
- Qu, T., H. Mitsudera, and T. Yamagata (1998), On the western boundary currents in the Philippine Sea, *J. Geophys. Res.*, *103*, 7537–7548.
- Qu, T., H. Mitsudera, and T. Yamagata (1999), A climatology of the circulation and water mass distribution near the Philippine Coast, *J. Phys. Oceanogr.*, *29*(7), 1488–1505.
- Qu, T., H. Mitsudera, and T. Yamagata (2000), Intrusion of the North Pacific waters into the South China Sea, *J. Geophys. Res.*, *105*, 6415–6424.
- Qu, T., Y. Du, and H. Sasaki (2006), South China Sea throughflow: A heat and freshwater conveyor, *Geophys. Res. Lett.*, *33*, L23617, doi:10.1029/2006GL028350.
- Qu, T., T. L. Chiang, C. R. Wu, P. Dutrieux, and D. Hu (2012), Mindanao Current/Undercurrent in an eddy-resolving GCM, *J. Geophys. Res.*, *117*, C06026, doi:10.1029/2011JC007838.
- Ray, R. D. (1998), Ocean self-attraction and loading in numerical tidal models, *Mar. Geod.*, *21*, 181–192.
- Rojana-Anawat, P., S. Pradit, N. Sukramongkol, and S. Siriaksophon (2000), Temperature, salinity, dissolved oxygen and water Masses of Vietnamese waters, in *Proceeding of the Fourth Technical Seminar on Marine Fishery Resources Survey in the South China Sea, Area IV: Vietnamese Waters*, pp. 291–307.
- Sasaki, H., M. Nonaka, Y. Masumoto, Y. Sasaki, H. Uehara, and H. Sakuma (2008), An eddy-resolving hindcast simulation of the quasiglobal ocean from 1950 to 2003 on the Earth Simulator, in *High Resolution Numerical Modelling of the Atmosphere and Ocean*, edited by K. Hamilton and W. Ohfuchi, chap. 10, pp. 157–185, Springer, N. Y.
- Shchepetkin, A. F., and J. C. McWilliams (2005), The Regional Ocean Modeling System: A split-explicit, free-surface, topography following coordinates ocean model, *Ocean Modell.*, *9*, 347–404.
- Takikawa, T., J. H. Yoon, and K. D. Cho (2005), The Tsushima warm current through Tsushima Straits estimated from ferryboat ADCP data, *J. Phys. Oceanogr.*, *35*, 1154–1168.
- Wang, L., and J. Gan (2014), Delving into three-dimensional structure of the West Luzon Eddy in a regional ocean model, *Deep Sea Res., Part I*, *90C*, 48–61, doi:10.1016/j.dsr.2014.04.011.
- Wu, C. R., and Y.-C. Hsin (2012), The forcing mechanism leading to the Kuroshio intrusion into the South China Sea, *J. Geophys. Res.*, *117*, C07015, doi:10.1029/2012JC007968.
- Xue, H., F. Chai, N. Pettigrew, D. Xu, M. Shi, and J. Xu (2004), Kuroshio intrusion and the circulation in the South China Sea, *J. Geophys. Res.*, *109*, C02017, doi:10.1029/2002JC001724.
- Yaremchuk, M., and T. Qu (2004), Seasonal variability of the large-scale currents near the coast of the Philippines, *J. Phys. Oceanogr.*, *34*, 844–855.
- Zu, T., J. Gan, and S. Y. Erofeeva (2008), Numerical study of the tide and tidal dynamics in the South China Sea, *Deep Sea Res., Part I*, *55*, 137–154, doi:10.1016/j.dsr.2007.10.007.